Available online at www.sciencedirect.com
SCIENCE DIRECT®
Journal of Theoretical Biology 222 (2003) 247–259
Journal of Theoretical Biology
www.elsevier.com/locate/jtbi

Simulating convergent extension by way of anisotropic differential adhesion

Mark Zajac[a,*], Gerald L. Jones[a], James A. Glazier[b]

[a] Department of Physics, University of Notre Dame, 225 Nieuwland Science Hall, Notre Dame, IN 46556, USA
[b] Department of Physics, 117 Swain Hall West, 727 East 3rd Street, Bloomington, IN 47405, USA

Received 27 June 2002; accepted 12 December 2002

Abstract

Simulations using the Extended Potts Model suggest that anisotropic differential adhesion can account for convergent extension, as observed during embryonic development of the frog *Xenopus laevis* for example. During gastrulation in these frogs, convergent extension produces longitudinal tissue growth from latitudinal elongation and migration of aligned constituent cells. The Extended Potts Model employs clustered points on a grid to represent subdivided cells with probabilistic displacement of cell boundaries such that small changes in energy drive gradual tissue development. For modeling convergent extension, simulations include anisotropic differential adhesion: the degree of attachment between adjacent elongated cells depends on their relative orientation. Without considering additional mechanisms, simulations based on anisotropic differential adhesion reproduce the hallmark stages of convergent extension in the correct sequence, with random fluctuations as sufficient impetus for cell reorganization.

Keywords: Convergent extension; Differential adhesion; Computer simulations; Energy minimization

1. Introduction

Three disparate examples show that cell statics and dynamics often depend on anisotropic differential adhesion: a discernible orientation for each cell accompanied by non-uniform stickiness over cell surfaces. First, in vertebrate (Armstrong, 1989) and invertebrate embryos, flat epithelial cells are only sticky on one side and organize to form stable cavities with nonadhesive cell surfaces facing the interiors of ducts, lumens and vacuoles. Second, as an isolated cell migrates over an artificially prepared surface, it reaches ahead, at the leading edge, and takes hold of the substrate using tendrillous filopodia (Huttenlocher et al., 1995; Lauffenburger and Horwitz, 1996) or wide flat lamellipodia which provide traction as the cell body moves forward, with adhesion necessarily undone at the trailing edge (Mitchison and Cramer, 1996), as the cell advances. Third, the "cell–cell traction" model (Keller et al., 2000) suggests anisotropic differential adhesion as a mechanism for longitudinal tissue extension, resulting from latitudinal cell convergence, with tightly bound lateral surfaces of adjacent cells parting when the narrow end of an advancing cell intervenes. As these examples illustrate, cell migration and organization often correlates with cell shape and non-uniform adhesion.

Direct observation (Keller et al., 1989; Shih and Keller, 1992b) of convergent extension does not reveal the cause of attendant cell reorganization. However, analytic calculations (Zajac et al., 2000) suggest that anisotropic differential adhesion can account for cell elongation, alignment and convergence, followed by tissue extension. The Extended Potts Model provides a more realistic implementation of the same basic hypothesis by treating each cell as an assembly of small rearrangeable pieces, allowing for cells with less restricted shapes and orientations. The model employs only random boundary deformations, governed almost entirely by non-uniform surface interactions between oriented, neighboring cells. Over time, perturbation of cell contacts gradually replaces weaker attachments with stronger attachments, tending towards a stable configuration of minimal energy. These simulations establish anisotropic differential adhesion as a sufficient condition for convergent extension without detailed consideration of any other intracellular or extracellular influences.

*Corresponding author.
E-mail address: mzajac@alumni.nd.edu (M. Zajac).

0022-5193/03/$ - see front matter © 2003 Elsevier Science Ltd. All rights reserved.
doi:10.1016/S0022-5193(03)00033-X

1.1. Empirical foundation

The development of animals with organs and internal cavities often includes convergent extension in which tissues grow longer and narrower to form axial structures. One example is the onset of digestive tract formation in sea urchins (Hardin and Cheng, 1989). Fruit fly development provides two more examples: telescopic leg growth (Condic et al., 1991) and an observed flow of surface tissue from the belly to the back (Irvine and Wieschaus, 1994), past the tail end of the embryo. Among the many other instances (Keller et al., 2000) of convergent extension, the frog *Xenopus laevis* may provide the most thoroughly documented example (Elul et al., 1997; Keller and Hardin, 1987; Keller and Shih, 1995; Winklbauer and Nagel, 1991; Wolpert et al., 1998).

Comparing all stages of *Xenopus laevis* development, gastrulation exhibits the most sweeping tissue rearrangements. The greatest changes (Keller et al., 1991) take place during convergent extension, when active cells elongate, align and then intercalate, generating longitudinal embryo growth from latitudinal cell migration. Elongation occurs first, leading to crudely rectangular shapes for cells that start out (Fig. 1a) roughly square. Soon after, alignment develops, resulting in a common orientation for the long axes of all cells. Somewhat later, intercalation (Fig. 1b) augments tissue length in the same way that merging two decks of cards produces a single, deeper stack. This specific three-fold process of elongation, alignment and intercalation is sometimes referred to as "mediolateral intercalation behavior" since "convergent extension" may also describe similar tissue deformations (Keller et al., 2000) driven by other mechanisms such as cell growth or radial cell migration.

Note the distinction between "elongation" and "extension" which describe increased aspect ratios for individual cells or entire tissues, respectively. Elongation alone would produce tissue extension in the same direction as the long axes of aligned constituent cells. However, intercalation yields increased tissue length (Fig. 1c) at right angles to the direction of cell elongation and migration. Thus, quite remarkably, extension develops with the long axis of each cell oriented at right angles to the long axis of the tissue. Consequently, convergent extension exhibits a pair of hallmark biaxial symmetries: one for cells and one for tissues.

A number of factors may influence convergent extension during undisturbed embryonic development but cultured tissues (Fig. 2) offer a simpler situation that is more amenable to analysis and simulation. Evidence suggests that convergent extension within *Xenopus laevis* embryos can be triggered by tissue layers below (Shih and Keller, 1992b), guided by tissue layers above (Winklbauer and Nagel, 1991) or channeled by stiff tissue blocks on either side (Keller et al., 1989). Previous theories have required at least one of these boundary conditions in order to explain convergent extension. For example, one model (Jacobson and Moury, 1995) proposes that cells within the extending tissue elongate while migrating to achieve increased contact with bounding tissues, on either side. However, excised monolayers of tissue (Shih and Keller, 1992a) display all the noted hallmarks of convergent extension, though isolated from any influence of adjacent tissues that might occur in undisected embryos. The shape changes of these cultured tissues and their constituent cells develop without influence from anisotropy of the surroundings. This convergent extension of excised tissues, in the absence of any obvious cues from the environment, invites an explanation in terms of collective behavior arising from intrinsic cell properties. Anisotropic differential adhesion provides a possible cause for the noted biaxial symmetries of both

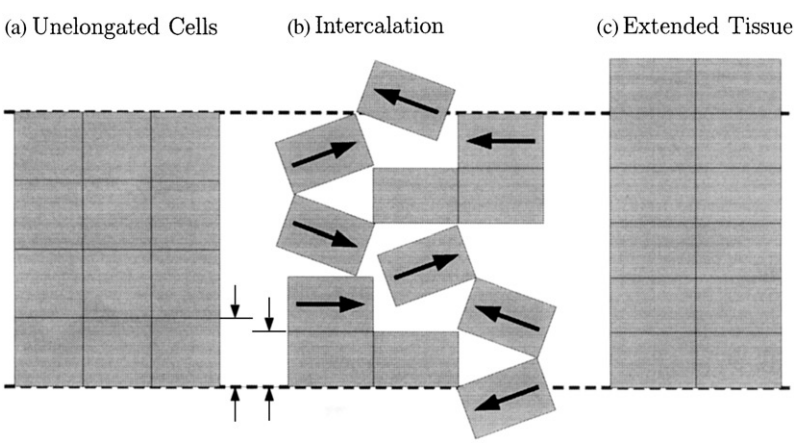

Fig. 1. Convergent extension schematically. Cells elongate (b) and then converge (arrows) to yield a longer (c) narrower tissue. Cells maintain roughly constant volume. The actual process (Fig. 2) does not include noticeable gaps between cells.

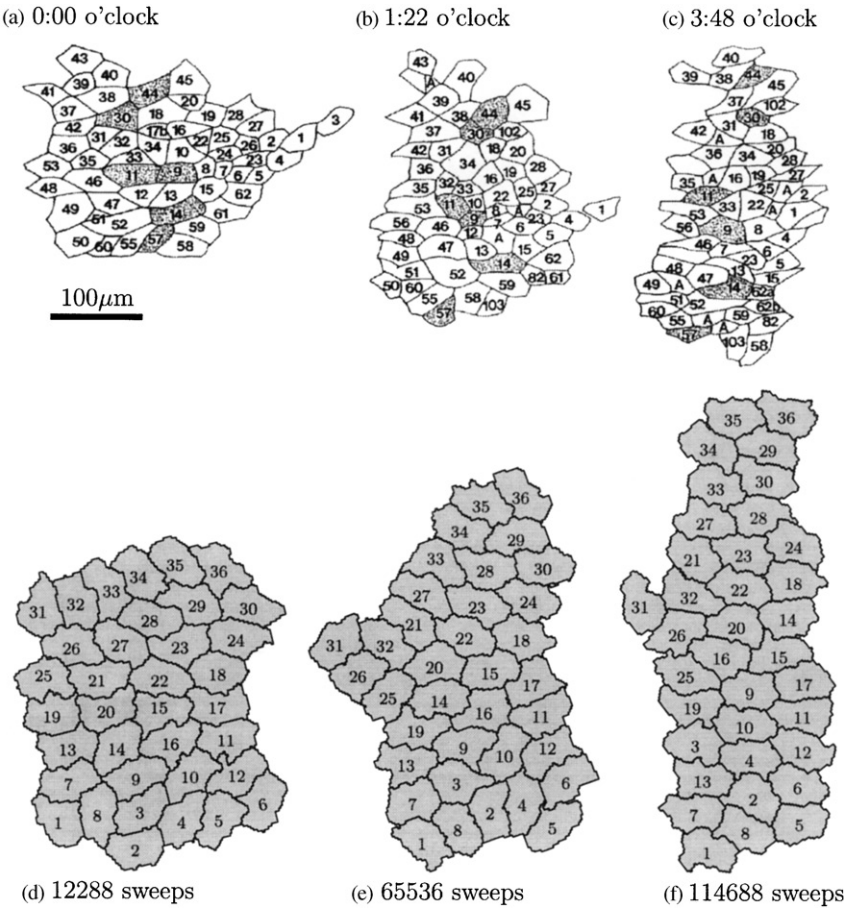

Fig. 2. Real and simulated convergent extension. Cell tracings (a–c) show cultured tissue, excised from the back of a *Xenopus laevis* embryo at stage 10.5 of development. Shading emphasizes separation of initially adjacent cells. Both real and simulated (d–f) tissues develop extension, over time. Contrary to overall alignment, cells at the narrow ends of some arrays point inwards from the boundary. Out of many experiments and simulations, the results shown here were chosen unscientifically on the basis of strong qualitative resemblance with no detailed correspondence of length or time-scales implied. The empirical results are reproduced (Shih and Keller, 1992a) by permission of The Company of Biologists Limited.

individual cells and whole tissues, during convergent extension.

1.2. Simulation preview

The Extended Potts Model belongs to a class of simulations (Agarwal, 1995b; Goel et al., 1970; Goel and Rodgers, 1978; Rogers and Goel, 1978) that subdivide cellular patterns by superimposing a grid, often termed a lattice, with probabilistic dynamics for pattern elements, reflecting changes in stored energy. Developed to investigate (Glazier and Graner, 1993; Graner and Glazier, 1992) spontaneous segregation of aggregated cells from different tissues, the model confirms all predictions of the (isotropic) Differential Adhesion Hypothesis (Steinberg, 1962a,b, 1963) which asserts that an energy gradient (Graner, 1993) drives rearrangement of mixed aggregates as cells shift positions to find more amenable coupling partners. Random membrane fluctuations provide a means of egress from marginally stable cell configurations. Later enhancements of the basic model include coupling to continuum models for chemical signaling (Agarwal, 1993, 1994; Jiang, 1998; Savill and Hogeweg, 1997) along with incorporation of mitosis (Mombach et al., 1993; Stott et al., 1999) for modeling tissue growth and cancer.

Simulations employ uniquely labeled domains (Fig. 3a) of clustered lattice sites to represent individual cells, with a second label (Fig. 3b) for each domain, shared by all cells from the same tissue. Distinguishing unlike cells allows for differential adhesion, reflected in suitably adjusted energies for each unit of contact at domain boundaries. Lattice patterns evolve by conditional, random transfer of boundary sites between neighboring domains, with automatic acceptance of modifications that reduce energy while the probability of acceptance falls exponentially for energy gains. Though deformable, each domain has a size constraint so that no cell can grow or shrink without bound.

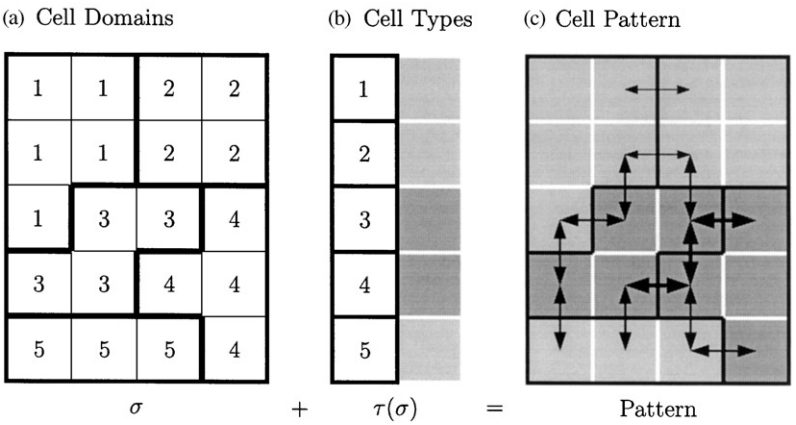

Fig. 3. Cell patterns on a lattice. A cell array σ together with a type list τ define a pattern. Domains of clustered sites define boundaries (thick lines, a) between cells. The strength of coupling (arrows, c) depends on the type (b) of cells at an interface.

Introducing anisotropic differential adhesion to the Extended Potts Model allows a novel approach (Zajac, 2002) to simulating convergent extension. Despite a constraint on overall shape, cells remain deformable, unlike other models for anisotropy (Drasdo et al., 1995; Goel and Leith, 1970) based on less flexible, more approximate cell shapes. Tracking the spatial distribution of sites within each lattice domain allows anisotropic binding based on the relative orientation of elongated neighboring cells. Under the Extended Potts Model, biaxial symmetry arises from these anisotropic cell interactions, rather than following from special boundary conditions, as assumed by an earlier model (Weliky et al., 1991) for convergent extension. The same earlier model requires persistent, directed cell motion rather than the simpler, random fluctuations, of the Extended Potts Model. In simulations, anisotropic differential adhesion proves sufficient as the sole mechanism for cell elongation and alignment followed by tissue extension.

2. Method

By treating each cell as an assembly of small rearrangeable pieces, the Extended Potts Model allows for elongated cells with measurable orientations while the statistical mechanics of interacting particles lends itself to a method for energy minimization based on a series of small perturbations. Early alternatives (Goel et al., 1970; Goel and Leith, 1970; Goel and Rodgers, 1978) considered mosaics of rigid congruent polygons, effectively using a single lattice site for each cell. However, using domains of clustered sites (Agarwal, 1993, 1995a,b; Glazier and Graner, 1993; Graner and Glazier, 1992; Upadhyaya, 2000) allows for more realistic cell shapes. Lattice site coupling at domain boundaries (Fig. 3c) models cell adhesion.

Based on experiments with thin sheets of excised tissue (Shih and Keller, 1992a), convergent extension simulations consider a single layer of cells, in two dimensions. Tracking cell orientations provides each cell with an intrinsic coordinate system, allowing for stickiness to vary as a function of location, over the surface of each cell. Size and shape constraints for each cell model limited compressibility and intracellular forces. In general, an evolving lattice pattern need not resemble a collection of cells but pattern energy in simulations reflects cell properties such that the probabilistic dynamics favor holding domains together as they deform and translate.

2.1. Pattern energy

Simulations characterize cell patterns in terms of stored energy. Rather than confronting anisotropic differential adhesion immediately, consider the simpler case of mixed, uniformly adhesive cells from different types of tissue with unlike cells distinguished by different degrees of stickiness. Contributions to the total pattern energy include a sum for coupling between cells and a sum reflecting limited cell compressibility:

$$E = \sum_{i,j,k,l}^{\text{sites}} (1 - \delta_{\sigma_{ij},\sigma_{kl}}) J_{\tau(\sigma)\tau(\sigma')} + \sum_{\sigma}^{\text{cells}} \lambda_{\tau(\sigma)} (A(\sigma) - A_{\circ})^2, \quad (1)$$

with different couplings $J_{\tau(\sigma)\tau(\sigma')}$ for every possible pair of cell types where domain σ has type $\tau(\sigma)$ while σ_{ij} and σ_{kl} are sites from adjacent domains σ and σ' respectively. The first sum in Eq. (1) ranges over all site coordinates i and j with k and l as coordinates of nearby sites. Only mismatched neighboring sites contribute to cell coupling since $\delta_{\sigma,\sigma'}$ equals unity when σ equals σ' and vanishes otherwise. Consequently, the model realistically localizes all the stored energy for coupling between cells at domain boundaries.

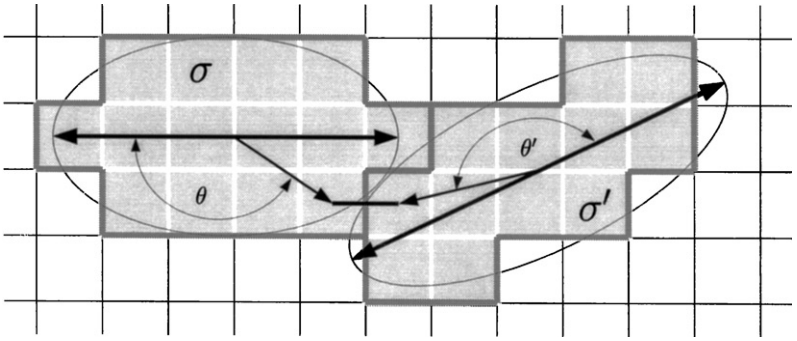

Fig. 4. Anisotropic binding. Coupling at the point of contact between cells σ and σ' depends on $\sin(\theta)$ and $\sin(\theta')$ with both θ and θ' in the interval $[0,\pi]$ so there is no need to distinguish between complementary angles.

The second sum in the pattern energy of Eq. (1) implements size constraints weighted by $\lambda_{\tau(\sigma)}$ for each cell. Working in two dimensions, the size constraints ensure an area close to $A_\circ$ for every cell, although the actual area $A(\sigma)$ for each cell fluctuates. By design, the size constraint increases pattern energy unless $A(\sigma)$ equals $A_\circ$ for all cells. Patterns usually include a wide border of lattice sites, assigned to a generalized cell of unlimited size, with $\lambda_{\tau(\sigma)}$ set equal to zero accordingly. This unique domain represents a nourishing culture medium surrounding the cells. Together, size constraints and distinctive couplings $J_{\tau(\sigma)\tau(\sigma')}$ for mismatched cells provide a sufficient description of pattern energy for isotropic differential adhesion, as in original simulations (Glazier and Graner, 1993; Graner and Glazier, 1992) of spontaneous cell sorting.

Simulations of convergent extension use modified coupling to introduce anisotropic differential adhesion. For an elongated cell, the principle axis (Appendix A) with the least moment of inertia gives the direction of elongation. Coupling becomes a function of vectors $\mathbf{r}$ and $\mathbf{r}'$ which locate a common boundary point (Fig. 4) relative to the respective centers of neighboring cells. These vectors have components (r,θ) and (r',θ') in polar coordinates with angles measured from the long axes of cells σ and σ', respectively. In terms of these variables, anisotropic coupling takes this form:

$$J(\mathbf{r},\mathbf{r}') = J_{\tau(\sigma)\tau(\sigma')} - \Delta(\mathbf{r})\Delta(\mathbf{r}'),$$
$$\Delta(\mathbf{r}) = \alpha_{\tau(\sigma)}\varepsilon(\sigma) r\sin(\theta), \qquad (2)$$

where $J_{\tau(\sigma)\tau(\sigma')}$ is just the coupling from Eq. (1) for uniformly sticky cells while $\Delta(\mathbf{r})$ and $\Delta(\mathbf{r}')$ describe contributions to anisotropy from cells σ and σ', respectively. The parameter $\alpha_{\tau(\sigma)}$ sets an upper limit on anisotropy with $\varepsilon(\sigma)$ as a measure of the cell elongation, derived (Appendix A) from the principle moments of inertia. For the unrealized case of perfectly elliptical cells, $\varepsilon(\sigma)$ reduces to the eccentricity. Simulations describe convergent extension within a block of cells from the same tissue so $\tau(\sigma)$ serves only to distinguish these cells from the surrounding culture medium. The anisotropy $\alpha_{\tau(\sigma)}$ is positive for coupling between cells but vanishes otherwise so that coupling to the culture medium does not depend on cell orientation. Substitution of $J(\mathbf{r},\mathbf{r}')$ for $J_{\tau(\sigma)\tau(\sigma')}$ in the pattern energy of Eq. (1) brings anisotropic differential adhesion to the Extended Potts Model.

Though chosen, in part, for ease of implementation, the anisotropy described by Eq. (2) satisfies important empirical and theoretical considerations. Significantly, the $r\sin(\theta)$ factors that influence coupling allow for relative displacement of parallel neighboring cells along their common direction of elongation with little change in bond strength at points where the cells maintain overlap. This coupling scheme mimics, to some degree, the "cell–cell traction" model (Keller et al., 2000) for convergence, allowing cells to crawl over each other in opposite directions, with firm anchorage opposing transverse detachment. In addition, the anisotropic component of $J(\mathbf{r},\mathbf{r}')$ has a product form consistent with models (Agarwal, 1993; Steinberg, 1975; Zajac et al., 2000) that reflect plausible binding site densities on opposed surfaces of adjacent cells. What is more, the coupling expressed by Eq. (2) satisfies conditions (Zajac et al., 2000) for cell alignment and tissue extension, derived analytically using simplified models, which assume more regular cells with restricted orientations. Notably, simulations consistent with this analytic modeling have proven successful while preliminary alternative adaptations of the Extended Potts Model failed to produce convergent extension.

Along with anisotropic differential adhesion, convergent extension simulations include an additional constraint on cell shape, formally equivalent to the constraint on cell size from Eq. (1) but with $\kappa_{\tau(\sigma)}$, $I(\sigma)$ and $I_\circ$ replacing $\lambda_{\tau(\sigma)}$, $A(\sigma)$ and $A_\circ$, respectively. The actual moment of inertia $I(\sigma)$ for the constituent lattice sites of each cell may differ from the ideal moment of inertia $I_\circ$ for an elongated yet otherwise undistorted domain. In exact analogy with constraining cell size, the shape constraint gives increased pattern energy unless $I(\sigma)$ equals $I_\circ$ for all cells.

Working in two dimensions, the shape constraint favors elongated cells when $I_\circ$ is set equal to the moment of inertia for a flat elliptical cell about an axis through the center of mass, perpendicular to the plane of the lamina:

$$I_\circ = \frac{A_\circ}{4}(a^2 + b^2),$$
$$A_\circ = \pi ab, \tag{3}$$

where a and b are the semimajor and semiminor axes of the ellipse, respectively. Adding this shape constraint to the pattern energy in Eq. (1) requires an additional sum over all domains, augmenting the sum that implements size constraints.

For a deformable cell, regulating $I(\sigma)$ alone does not guarantee a convex shape or even preclude an annular distribution of mass which is completely unrealistic. However, in two dimensions, the shape constraint of Eq. (3) strongly favors elongated cells when combined with the size constraint and positive cell couplings, which yield lower energies for minimal surfaces. The shape constraint is meant to crudely model intracellular forces such as cytoskeletal effects which, in principle, might either promote or retard cell elongation under anisotropic differential adhesion. For unequal values of a and b the shape constraint favors elongated cells while favoring circular cells when a and b are chosen equal.

2.2. Pattern dynamics

The Extended Potts Model does not attempt to capture the internal mechanics of individual cells. Instead, the model assumes that a local energy gradient sets the direction of migration for each cell (Graner, 1993) while a global energy minimum identifies the final destination. Random fluctuations allow cells to escape from local minima but need not reflect actual trajectories. The idea is that differential adhesion and energy minimization give the correct sequence of events during cell reorganization, just as topography orders the gates of a slalom course without recognizing that skiers have muscles, which allow for autonomous steering.

Lattice patterns evolve gradually through repeated acceptance or rejection of cell shape perturbations, governed by small changes in pattern energy. For each attempt at pattern modification, a lattice site is chosen at random and provisionally altered to match the sites in a different, randomly selected domain, thus transferring the chosen site to the selected domain, on a trial basis. However, in a departure from the usual Metropolis dynamics for lattice patterns (Gilks et al., 1996; Koonin and Meredith, 1990; Metropolis et al., 1953), cell simulations only consider sites at a boundary between domains for modification, with modified sites reassigned to the domain of a randomly selected nearby site, in the case of a successful trial. This scheme prevents instantaneous transfer of cell fragments to distant locations, including the insertion of a fragment from one cell at the heart of another. Changes are both local and localized at cell boundaries which makes sense for simulations of cells with random membrane fluctuations.

Each attempted lattice modification causes a slight change in pattern energy which depends on modified contact between cells, influenced by the size and shape constraints. Decreases in pattern energy are always accepted, while the likelihood of accepting an energy increase depends on a ratio of Boltzmann factors:

$$P(\Delta E) = \begin{cases} \dfrac{e^{-E_1/T}}{e^{-E_0/T}} & \text{for } E_1 > E_0, \\ 1 & \text{for } E_1 \leqslant E_0, \end{cases} \tag{4}$$

where $P(\Delta E)$ is the probability of accepting a change in energy from E_0 to E_1 while T is the temperature, measured in units of energy. In these simulations, adjusting T simply determines the average acceptable energy increase for pattern modifications and does not represent actual, thermodynamic temperature. For sufficiently low temperatures, the most likely patterns are small perturbations of a minimal energy configuration. Technically, this variant of the usual Metropolis dynamics does not have (Zajac et al., 2000) microscopic reversibility (Meyer, 2000) as required for true, thermal equilibrium statistics. However, successive lattice modifications do meet the definition of an ergodic Markov process (Gilks et al., 1996) which is sure to reach a steady state, eventually. Notice that convergent extension belongs to a transient phase of this Markov process, neglected in more familiar Metropolis calculations of ensemble averages, at thermal equilibrium.

Though uncomplicated in principle, anisotropic coupling between cells is not simple to implement. For elongated cells, anisotropic differential adhesion from Eq. (2) depends on polar coordinates r and θ for each boundary site, measured from the center of mass and the long axis (Fig. 4) respectively, for each cell. As an advancing cell gains one lattice site from a retreating neighbor the centroid and orientation (Appendix A) of each changes slightly. It follows that coupling changes at all points where either of the altered domains contacts any adjacent cell, not just at points in the neighborhood of a single modified site.

Rather than laboriously updating polar coordinates for all lattice sites at multiple cell boundaries whenever a single site changes, current simulations replace individual site coordinates r and θ with average values for segments of contact between adjacent cells. Consequently, updated coupling requires a visit to each boundary segment, rather than visiting each boundary site, for a modified cell pair. This faster algorithm for anisotropic differential adhesion meets the same analytic guidelines (Zajac et al., 2000) as the coupling described

by Eq. (2) and may be regarded as an approximation of the original scheme or simply adopted as an alternative.

3. Results

In an archetypal simulation, the Extended Potts Model yields a correct ordering of time-scales for convergent extension, starting from a roughly square block (Fig. 5a) of weakly elongated, randomly oriented cells. Full cell elongation develops (Fig. 5a and b) almost immediately with tissue extension building (Fig. 5d–f) more gradually. Soon after elongation, alignment begins to develop, leading, with relatively little delay, to a point (Fig. 5c) beyond which the directions for tissue extension and overall alignment remain fairly perpendicular, the salient feature of convergent extension. For the results shown here, a large jump in alignment (Fig. 5e and f) occurs when cells at the narrow ends of the array swing round to acquire the common orientation of bulk cells. These simulation results demonstrate that anisotropic differential adhesion offers a plausible explanation for cell elongation followed by alignment and then tissue extension.

Results include quantitative measures (Appendix A) of elongation, alignment and extension, plotted against time. The aspect ratio of a cell array gives the degree of extension, starting at one, for a squarish array, and increasing as the length grows, relative to the width, until full extension is reached. In reporting average

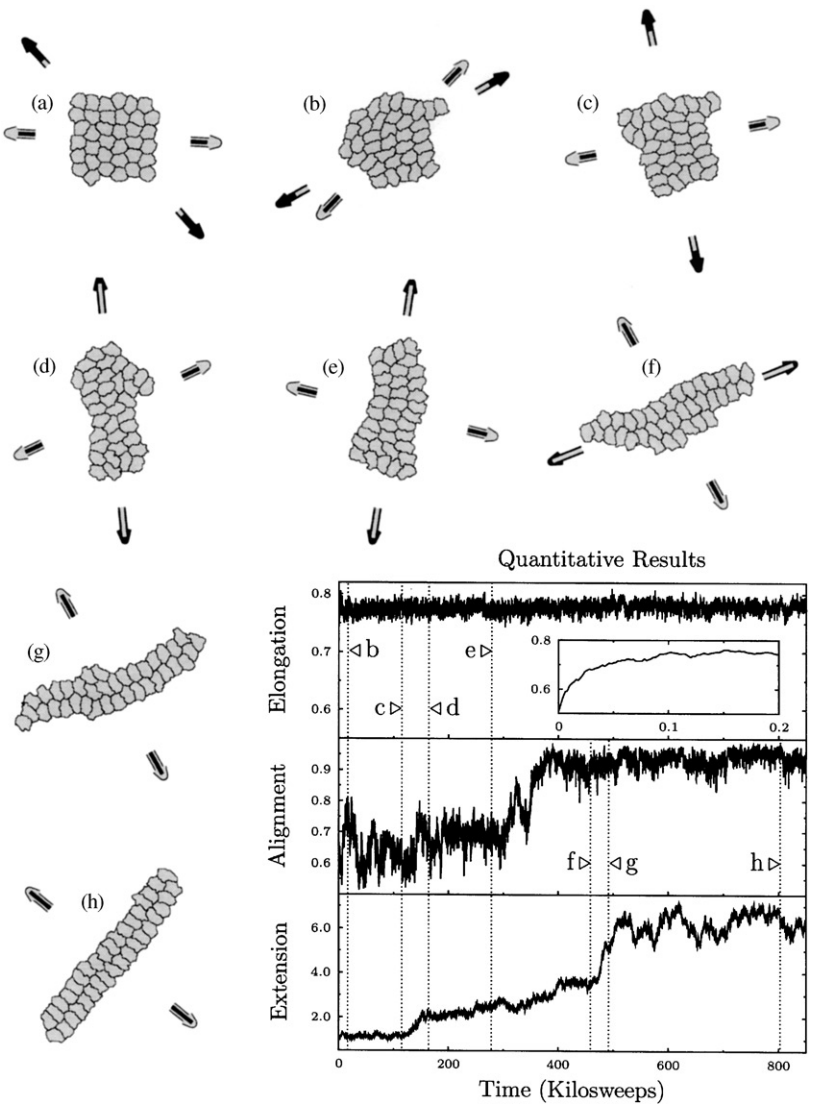

Fig. 5. Elongation before alignment before extension, in simulations. Excluding the initial condition (a), each stage (b–h) corresponds to a vertical, dotted line on graphs of extension, alignment and elongation (all dimensionless) versus time (measured in thousands of sweeps) with an inset showing rapid early elongation. Dark arrows (a–f) show the direction of extension while light arrows (a–h) show overall alignment with contrasting overlays showing magnitude or degree, in both cases.

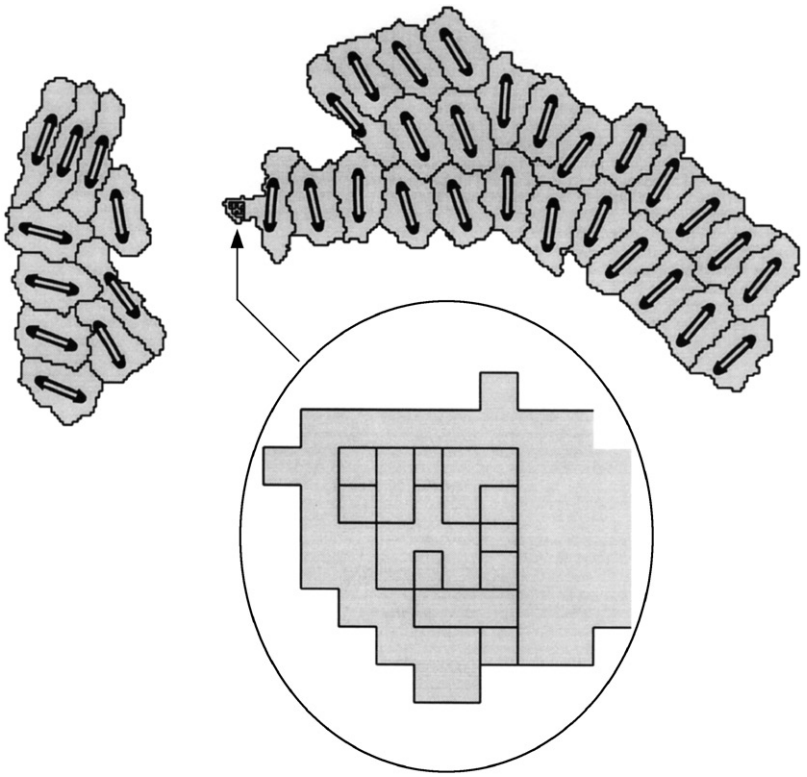

Fig. 6. Disastrous coupling. Excessive anisotropy in Eq. (2) yields negative coupling at domain boundaries which drives cells to hyperelongate, commingle (magnified) and pull apart, all to reduce stored energy. For each cell σ the upper limit on anisotropy $\alpha_{\tau(\sigma)}$ must be chosen to avoid such disasters.

elongation, the aspect ratio of each cell is converted into the eccentricity of an equivalent ellipse. Consequently, elongation starts at zero for circular cells, and increases towards one, as cells lengthen. Alignment ranges from $1/2$ for cells with utterly random orientations up to one for cells with a single, common orientation. Both extension and alignment are quadratically sensitive to any curvature (Fig. 7a) of a long narrow cell array. Time is measured in sweeps of the lattice with the number of pattern modifications attempted in one sweep equal to the number of lattice sites.

In agreement with analytic modeling (Zajac et al., 2000), the degree of tissue extension, in simulations, depends on the degree of anisotropy for binding between cells. Extension increases as the difference between maximum and minimum coupling in Eq. (2) increases. Simulations that yield two, adjacent columns of cells (Fig. 5h) employ a relative difference of 57% between binding for aligned and unaligned cells. Anisotropy of less than 35% yields little or no extension while anisotropy of more than 65% consistently leads to a single column of cells. These numbers are not especially meaningful, due to qualitative implementation of non-uniform cell adhesion. Even so, simulations describe not only extension that ends with more than one column of cells, as in *Xenopus laevis*, but, with increased anisotropy, also allow further convergence, ending with a single column of cells, as in ascidians (Munro and Odell, 2002).

Suitably adjusted simulation parameters suppress a pair of unrealistic outcomes. First, as implemented, convergent extension simulations under the Extended Potts Model depend on positive coupling at domain boundaries to maintain compact cells (Upadhyaya, 2000; Zajac, 2002). Excessive anisotropy (Fig. 6) in the coupling of Eq. (2) can lead to disastrous negative values, causing cell disintegration as domains commingle in order to decrease stored energy through increased coupling of mismatched lattice sites. Second, with insufficient cohesion, cell arrays sometimes develop unnatural curvature (Fig. 7a) or a spurious branch (Fig. 7b) during extension. Adjusting cell couplings $J_{\tau(\sigma)\tau(\sigma')}$ in Eq. (2) to increase the work of separating attached cells solves, or at least mitigates, the problem. The catastrophe of negative coupling is an artificial pitfall with no biological counterpart but successful adjustment of adhesion to prevent spurious branches and cell array curvature, in simulations, shows that adhesion can regulate tissue geometry during convergent extension.

The constraint on cell shapes allows two extreme alternatives for bulk treatment of unspecified intracellular forces, in simulations. Setting the shape constraint to favor circular cells represents a case for which effects

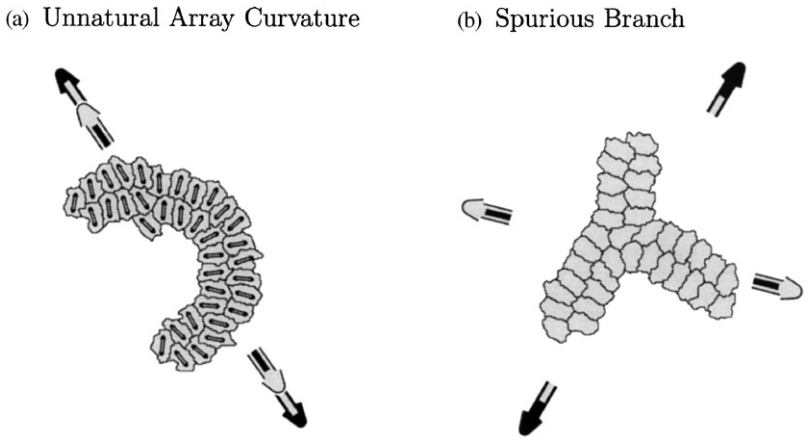

Fig. 7. Insufficient cohesion. Relatively weak binding between cells allows increased contact with the surroundings leading to curvature (a) or even spurious branches (b) instead of realistic convergent extension. With curvature, the opposite ends of an array come closer together, which detracts from extension, while the difference in orientation between distant cells ruins overall alignment, despite nearly identical orientations for neighbors.

such as membrane elasticity tend to hinder elongation, keeping cells compact. Setting the shape constraint to favor elliptical cells represents a case for which effects such as active redistribution of the cytoskeleton tend to promote elongation. For either case, simulations with anisotropic differential adhesion yield roughly the same degree of cell elongation as long as adhesion and shape constraints make roughly equal contributions to changes in energy, for each attempt at pattern modification.

However, changing the weight of the shape constraint by an order of magnitude, more or less, has measurable consequences. Giving increased weight to the shape constraint makes cells more rigid and less able to slip past one another, curtailing alignment, convergence and extension. With the shape constraint weighted less strongly, cells readily converge, reorganizing to give more rows and fewer columns, but the resulting arrays are prone to curvature (Fig. 7a) which detracts from elongation and makes it harder to quantify alignment.

Notice that shape constraints alone can drive cell elongation but cell alignment and tissue extension, in simulations, require anisotropic differential adhesion as well. Cells are not drawn into the surrounding medium during convergent extension. Just the opposite is true. Increased contact with the medium represents wasted binding potential for exposed cell surfaces. Anisotropic differential adhesion promotes extension by compensating for increased tissue perimeter with stronger attachments for aligned cells. With no anisotropy, even elongated cells form compact clusters of minimal perimeter rather than extended configurations with longer boundaries. For example, three elongated cells with uniformly sticky surfaces arrange themselves into a crude, rounded triangle, in simulations. This understanding of simulated convergent extension agrees with the results (Zajac et al., 2000) of analytic modeling.

The outcome of convergent extension simulations depends on the amplitude of fluctuations in pattern energy. With roughly 46% acceptance of attempted lattice modifications (including automatic acceptance of modifications that yield reduced energy) simulations exhibit both cell alignment and tissue extension. However, increasing temperature in Eq. (4) to give 72% acceptance yields overactive cells which converge to give extension (Fig. 8a) but fail to settle on a common alignment. Alternatively, decreasing T to give 21% acceptance yields sluggish, inflexible cells which align (Fig. 8b) but fail to converge. Cells must escape local energy minima but not the global minimum that represents full extension.

4. Discussion

The Extended Potts Model shows that anisotropic differential adhesion can account for longitudinal tissue extension resulting from latitudinal elongation and convergence of aligned constituent cells. Quantitative measures of convergent extension, from simulations, suggest new analysis of tissue extension along with cell elongation and alignment, in experiments. Modeling further empirical details might enhance simulation realism, especially for cell dynamics, but the current level of simplicity allows unambiguous connection between cause and effect.

4.1. Critical evaluation

Convergent extension under the Extended Potts Model hinges on anisotropic differential adhesion, with no attempt at faithful reproduction of every biological detail. Displacement of cell boundaries follows from a gradual accumulation of local, random perturbations,

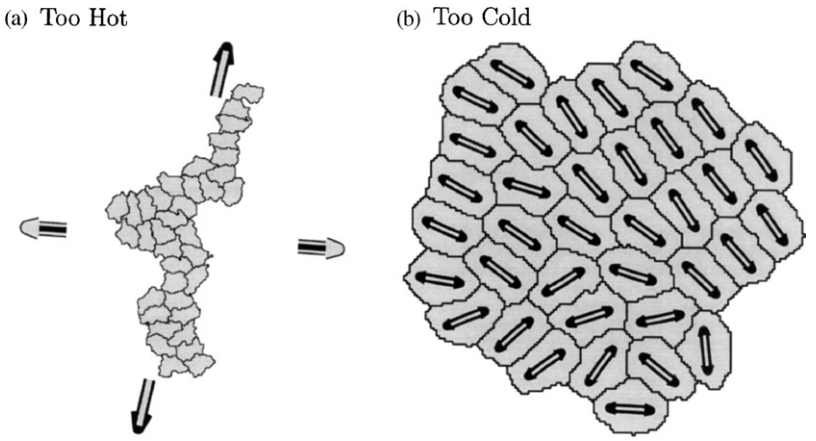

Fig. 8. Cell activity. At high temperatures, overactive cells (a) reorganize to give an extended array but overall alignment is poor, fluctuating wildly. At low temperatures, sluggish cells (b) develop elongation and alignment but otherwise fail to exhibit convergent extension.

neglecting any sophisticated locomotor apparatus that might drive real, living cells. The model does not include persistence of motion resulting from cytoskeletal rectification, for example. Focused on adhesion, simulations constrain the size and shape of each cell in a simplistic, bulk representation of all remaining cell properties, including limited compressibility and cytoskeletal effects. The size and shape constraints both act at the scale of entire lattice domains, leaving cell adhesion with unrealistic, full control over local boundary displacement, for each small segment of contact between cells.

Furthermore, though invoking adhesion to drive cell reorganization on the scale of tissues, simulations do not reflect the smaller scale details of cell binding, ignoring molecular dynamics, for example. Based on corresponding experiments, simulation consider isolated cell arrays which offer the simplicity of homogeneous boundary conditions. However, channeling by adjacent tissues in actual embryos might, for example, suppress the spurious branches and cell array curvature seen in failed (Fig. 7) simulations, relaxing current limits on parameter values that lead to acceptable (Fig. 5) results. Despite these many simplifications and approximations, Extended Potts Model simulations establish anisotropic differential adhesion as a sufficient condition for convergent extension, accounting for all its salient features with essentially one assumption.

4.2. Possible measurements

First and foremost, simulation results invite experiments designed to measure anisotropic differential adhesion between cells since modeling requires nothing more to explain convergent extension. Unfortunately, simulations do not distinguish an uneven distribution of cell adhesion molecules from localization of specialized anchorage mechanisms such as filopodia and lamellipodia. Consequently, simulations do not help to narrow the experimental search for anisotropic differential adhesion by suggesting a particular mechanism. However, simulated convergent extension does not follow from special boundary conditions or detailed understanding of intracellular biochemistry, which reduces the number of leads to follow.

Developed for simulations, quantitative measures (Appendix A) of elongation, alignment and extension are immediately applicable to existing (Keller et al., 1989, 2000) empirical data. For example, previously published cell tracings (Fig. 2a–c) are suitable for analysis using only readily available software for image capture and digitization with some very simple custom code for calculating the spatial distribution of pixels in each cell. A more complete time series of similar images would allow detailed comparison with results (Fig. 5) from simulations. This quantitative analysis of elongation, alignment and extension might be of interest in its own right even if anisotropic differential adhesion does not prove to be the cause of convergent extension.

Empirical data in a format that compares directly to simulated results could guide the search for good model parameters. Simulation results depend on parameters that govern cell size, cell shape and the amplitude of boundary fluctuations as well as a parameter for the degree of anisotropy in cell binding. Further parameters include energy densities for interfaces between cells as well as interfaces with the culture medium. Results for some extreme cases (Fig. 8a and b) set bounds on what simulations can hope to accomplish. However, systematic variation of each simulation parameter is not practical, since each simulation takes a long time (more than 72 h for one simulation at 750 MHz when averaging 14 cycles for each mathematical operation). Comparing simulations to suitably analysed empirical results could help to weed out parameter values that stray too far from reality. This feedback from experiments could be very illuminating, particularly for efforts to improve modeling of cell dynamics which currently have no empirical basis in simulations.

4.3. Final analysis

Adapted to cells with non-uniform stickiness, the Extended Potts Model supports a simple yet effective mechanism for convergent extension. Simulations capture cell elongation and alignment, followed by tissue extension with anisotropic differential adhesion between oriented neighboring cells as the only major assumption. Distinctive cell and tissue geometries originate with the surface adhesion properties of each cell rather than from special boundary conditions at the edge of an extending tissue. Success does not hinge on detailed knowledge of cellular dynamics or internal biochemistry. Results include useful quantitative measures of convergent extension. Simulations based on anisotropic differential adhesion alone give elongation, alignment and extension in the correct order, with random fluctuations as sufficient impetus for cell reorganization.

Appendix A

Quantitative measures of convergent extension should reflect the hallmark biaxial symmetries of both converging cells and extending tissues. However, in simulations, cell and tissue patterns must not be tied to symmetries of the underlying lattice. Switching from the artificially imposed axes of lattice coordinates to the naturally occurring symmetry axes of cells and tissues hinges on the transformation properties (Smith, 1984) of real symmetric matrices. Eigenvalues and eigenvectors (Arfken, 1985) give magnitude and direction for elongation, alignment and extension.

A.1. Elongation and extension

For a rectangular arrangement of cells, the direction of extension coincides with an axis such that the total mass is evenly balanced on either side, with the narrowest possible distribution. Without fail, a second, perpendicular axis then has the widest possible evenly balanced distribution of mass with no correlation between mass distributions about the two axes. The relative width of these two distributions gives the aspect ratio for the cell array, reported as the degree of extension. Applied to individual cells, the same analysis gives orientation and elongation. However, an extra step converts the aspect ratio of each cell into the eccentricity of an equivalent ellipse. Consequently, elongations range from zero, for circular cells, up to one, as cells become increasingly oblong. These definitions for extension and elongation reflect general properties of the inertia tensor (Goldstein, 1980) for any rigid body.

In detail, moments of inertia (Fowlse, 1985; Goldstein, 1980) about the center of mass serve to quantify both elongation of individual cells and extension of entire cell arrays. Therefore, calculations of elongation and extension are formally equivalent. On a regular lattice, using the row and column indices of each site as Cartesian coordinates provides a basis for calculating inertia tensor matrix elements:

$$
\begin{aligned}
I_{xx} &= \sum_{i=1}^{N} (y_i - \bar{y})^2, \\
I_{xy} &= -\sum_{i=1}^{N} (x_i - \bar{x})(y_i - \bar{y}), \\
I_{yx} &= I_{xy}, \\
I_{yy} &= \sum_{i=1}^{N} (x_i - \bar{x})^2,
\end{aligned}
\tag{A.1}
$$

where each sum visits N sites at coordinates (x_i, y_i) with $(\bar{x}, \bar{y})$ as average values which give the center of mass. The sums may be restricted to the sites from a single cell, when calculating elongation, or expanded to include the sites from all cells when calculating extension. In general, these elements of the inertia tensor do not uniquely determine the geometry of a rigid body, but coupling and constraints combine to ensure compact, elongated yet otherwise irregular shapes, resembling cells from experiments.

Describing each irregular, elongated cell in terms of an equivalent elliptical lamina, the principle axes (Goldstein, 1980) and corresponding moments of inertia give orientations and lengths for the semimajor and semiminor axes. In two dimension, simple algebraic formulae yield the desired eigenvalues and eigenvectors:

$$
\lambda_b = \tfrac{1}{2}(I_{xx} + I_{yy}) + \tfrac{1}{2}\sqrt{(I_{xx} - I_{yy})^2 + 4I_{xy}^2}, \tag{A.2}
$$

$$
\mathbf{b} = \hat{\mathbf{x}} I_{xy} + \hat{\mathbf{y}}(\lambda_b - I_{xx}), \tag{A.3}
$$

where λ_b is the *larger* eigenvalue so that the corresponding eigenvector $\mathbf{b}$ points along the *semiminor* axis with unit vectors $\hat{\mathbf{x}}$ and $\hat{\mathbf{y}}$ along rows and columns of the lattice, respectively. Changing the sign of the radical in the first equation gives the smaller eigenvalue λ_a which yields the corresponding eigenvector $\mathbf{a}$ when substituted for λ_b in the second equation. The eigenvectors are unnormalized.

Shifting to the principle axis coordinate system, direct calculation shows that $2\sqrt{\lambda_b}$ is the length of the semimajor axis, for the equivalent elliptical cell, without loss of generality. Eccentricity follows immediately from the ratio of the eigenvalues:

$$
\varepsilon = \sqrt{1 - \lambda_a/\lambda_b}, \tag{A.4}
$$

with ε ranging from zero for a circle to one for an infinite line. For a single cell, ε and $\mathbf{a}$ are referred to as elongation and orientation, respectively. However, when calculated for an array of cells, $\mathbf{a}$ is referred to as the direction of extension with λ_b/λ_a as the magnitude,

refered to as the degree of extension or simply the extension.

A.2. Alignment

A good measure of alignment should distinguish randomly oriented cells from cells with parallel elongation and should also remain unchanged when $-\mathbf{a}$ replaces $\mathbf{a}$ as the orientation, for any cell. An alignment tensor A of rank two can meet the latter requirement by pairing components of the orientation vector for each cell in every possible quadratic combination:

$$A_{xx} = \frac{1}{N}\sum_{i=1}^{N} \cos^2\theta_i,$$

$$A_{xy} = \frac{1}{N}\sum_{i=1}^{N} \cos\theta_i \sin\theta_i,$$

$$A_{yx} = A_{xy},$$

$$A_{yy} = \frac{1}{N}\sum_{i=1}^{N} \sin^2\theta_i, \tag{A.5}$$

for an array of N cells where $\cos\theta_i$ and $\sin\theta_i$ are just the components of $\mathbf{a}$ for each cell, after normalization. It is not immediately obvious that this tensor can distinguish randomly oriented cells from cells with parallel elongation.

As a preliminary step, consider the determinant and the trace of the alignment tensor. As always, the determinant (Arfken, 1985; Smith, 1984) does not depend on the choice of coordinates and equals the product of the eigenvalues:

$$\begin{aligned}\det(A) &= A_{xx}A_{yy} - A_{xy}A_{yx}\\ &= \lambda_a\lambda_b,\end{aligned} \tag{A.6}$$

where $\det(A)$ is the determinant with A_{xx} and A_{yy} giving way to eigenvalues λ_a and λ_b under the orthogonal transformation such that A_{xy} and A_{yx} are eliminated. Furthermore, the trace $\mathrm{tr}(A)$ is also invariant and equals the sum of the eigenvalues:

$$\begin{aligned}\mathrm{tr}(A) &= A_{xx} + A_{yy}\\ &= \frac{1}{N}\sum_{i=1}^{N}(\cos^2\theta_i + \sin^2\theta_i)\\ &= \lambda_a + \lambda_b\\ &= 1,\end{aligned} \tag{A.7}$$

which does not depend on the choice of coordinate axes for individual cell orientations, as expected.

A pair of limiting cases now establish the largest eigenvalue of A as a good measure of alignment. For a totally random arrangement of cells, both A_{xx} and A_{yy} equal $1/2$ while A_{xy} and A_{yx} both vanish since $\cos^2\theta_i$ and $\sin^2\theta_i$ both average to $1/2$ for a uniform distribution of angles while the average of $\cos\theta_i\sin\theta_i$ vanishes. It follows that the largest eigenvalue of A is $1/2$ for the case of randomly oriented cells. For perfect alignment, with θ_i equal to the same fixed θ for all cells, $A_{xx}A_{yy}$ and $A_{xy}A_{yx}$ both reduce to $\cos^2\theta\sin^2\theta$ in which case $\det(A)$ vanishes. Consequently, one eigenvalue in the product $\lambda_a\lambda_b$ must equal zero. It follows that the largest eigenvalue equals one for the case of perfect alignment since the sum of the eigenvalues in Eq. (A.7) must equal unity. In summary, the largest eigenvalue of the alignment tensor falls in the interval $[1/2, 1]$ with a minimum for randomly oriented cells and a maximum for perfect alignment. Formulae for the largest eigenvalue from Eq. (6) and the corresponding eigenvector from Eq. (7) give $\mathbf{b}$ as the direction of alignment with λ_b as the magnitude, provided that A_{xx}, A_{xy} and A_{yy} replace I_{xx}, I_{xy} and I_{yy} respectively, in each formula.

References

Agarwal, P., 1993. Cell-based computer models in developmental biology. Ph.D. Thesis, New York University.

Agarwal, P., 1994. Simulation of aggregation in *Dictyostelium* using the cell programming language. Comput. Appl. Biosci 10 (6), 647–655.

Agarwal, P., 1995a. The cell programming language. Artif. Life 2 (1), 37–77.

Agarwal, P., 1995b. Cellular segregation and engulfment simulations using the cell programming language. J. theor. Biol. 176 (1), 79–89.

Arfken, G., 1985. Mathematical Methods for Physicists, 3rd Edition. Academic Press, Inc., Orlando, FL.

Armstrong, P.B., 1989. Cell sorting out: the self-assembly of tissues in vitro. Crit. Rev. Biochem. Mol. Biol. 24 (2), 119–149.

Condic, M., Fristrom, J., Fristrom, D., 1991. Apical cell shape changes during *Drosophila* imaginal leg disk elongation: a novel morphogenetic mechanism. Development 111, 23–33.

Drasdo, D., Kree, R., McCaskill, J.S., 1995. Monte Carlo approach to tissue-cell populations. Phys. Rev. E 52 (6), 6635–6657.

Elul, T., Koehl, M.A.R., Keller, R., 1997. Cellular mechanism underlying neural convergent extension in *Xenopus laevis* embryos. Dev. Biol. 191, 243–258.

Fowlse, G.R., 1985. Analytical Mechanics, 4th Edition. Saunders Golden Sunburst Series. Saunders College Publishing, London.

Gilks, W.R., Richardson, S., Spieglhalter, D.J. (Eds.), 1996. Markov Chain Monte Carlo in Practice. Chapman & Hall, Boca Raton, FL, USA.

Glazier, J.A., Graner, F., 1993. Simulation of differential driven adhesion rearrangement of biological cells. Phys. Rev. E 47 (3), 2128–2154.

Goel, N.S., Leith, A.G., 1970. Self-sorting of isotropic cells. J. theor. Biol. 28, 469–482.

Goel, N.S., Rodgers, G., 1978. Computer simulation of engulfment and other movements of embryonic tissues. J. theor. Biol. 71, 103–140.

Goel, N.S., Campbell, R., Rosen, R., Maritnez, H., Ycas, M., 1970. Self-sorting of isotropic cells. J. theor. Biol. 28, 423–468.

Goldstein, H., 1980. Classical Mechanics, 2nd Edition. Addison-Wesley Series in Physics. Addison-Wesley, Don Mills, Ontario.

Graner, F., 1993. Can surface adhesion drive cell rearrangement? Part I: biological cell-sorting. J. theor. Biol. 164, 455–476.

Graner, F., Glazier, J.A., 1992. Simulation of biological cell sorting using a two-dimensional extended Potts Model. Phys. Rev. Lett. 69 (13), 2013–2016.

Hardin, J.D., Cheng, L.Y., 1989. The mechanism and mechanics of archenteron elongation during sea urchin development. Dev. Biol. 115, 490–501.

Huttenlocher, A., Sandborg, R.R., Horowitz, A.F., 1995. Adhesion in cell migration. Curr. Opin. Cell Biol. 7, 697–706.

Irvine, K.D., Wieschaus, E., 1994. Cell intercalation during *Drosophila* germband extension and its regulation by pair-rule segmentation genes. Development 120 (4), 827–841.

Jacobson, A., Moury, J.D., 1995. Tissue boundaries and cell behavious during neurulation. Dev. Biol. 171, 98–110.

Jiang, Y., 1998. Cellular pattern formation. Ph.D. Thesis, University of Notre Dame, Notre Dame, Indiana.

Keller, R., Hardin, J., 1987. Cell behaviour during active cell rearrangement: evidence and speculations. J. Cell Sci. Suppl. 8, 369–393.

Keller, R., Shih, J., 1995. Cell and tissue behavior during convergence and extension of the embryonic axial mesoderm in the frog *Xenopus laevis*. In: Beysens, D., Forgacs, G., Gaill, F. (Eds.), Interplay of Genetic and Physical Processes in the Development of Biological Form. Les Houches Series. World Scientific, New York, pp. 143–153.

Keller, R., Cooper, M.S., Danilchik, M., Tibbetts, P., Wilson, Paul, A., 1989. Cell intercalation during notochord development in *Xenopus laevis*, J. Exp. Zool. 251, 134–155.

Keller, R., Shih, J., Wilson, P., 1991. Cell motility, control and function of convergence and extension during gastrulation of *Xenopus*. In: Keller, R., Clark Jr., W., Griffin, F. (Eds.), Gastrulation: Movements, Patterns and Molecules. Bodega Marine Laboratory, Marine Sciences Series 3. Plenum Press, New York, pp. 101–119.

Keller, R., Davidson, L., Edlund, A., Elul, T., Ezin, M., Shook, D., Skoglund, P., 2000. Mechanisms of convergence and extension by cell intercalation. Philos. Trans. R. Soc. B 355 (1399), 897–922.

Koonin, S.E., Meredith, D.C., 1990. Computational Physics (FORTRAN Version). Addison-Wesley, New York.

Lauffenburger, D., Horwitz, A.F., 1996. Cell migration: a physically integrated molecular process. Cell 84, 359–369.

Metropolis, N., Rosenbluth, M., Rosenbluth, A., Teller, A., Teller, E., 1953. Equation of state calculations by fast computing machines. J. Chem. Phys. 21, 1087–1092.

Meyer, P., 2000. Computational studies of pure and dilute spin models. Master's Thesis, School of Mathematics and Computing, University of Derby.

Mitchison, T.J., Cramer, L.P., 1996. Actin-based cell motility and cell locomotion. Cell 84, 371–379.

Mombach, J.C.M., de Almeida, R.M.C., Iglesias, J.R., 1993. Mitosis and growth in biological tissues. Phys. Rev. E 48 (1), 598–602.

Munro, E.M., Odell, G.M., 2002. Polarized basolateral cell motility underlies invagination and convergent extension of the ascidian notochord. Development 129, 13–24.

Rogers, G., Goel, N.S., 1978. Computer simulation of cellular movements: cell-sorting, cellular migration through a mass of cells and contact inhibition. J. theor. Biol. 71 (1), 141–166.

Savill, N., Hogeweg, P., 1997. Modeling morphogenesis: from single cells to crawling slugs. J. theor. Biol. 184 (3), 229–235.

Shih, J., Keller, R., 1992a. Cell motility driving mediolateral intercalation in explants of *Xenopus laevis*. Development 116 (4), 901–914.

Shih, J., Keller, R., 1992b. The epithelium of the dorsal marginal zone of *Xenopus laevis has organizer properties*. Development 116 (4), 887–899.

Smith, L., 1984. Linear Algebra 2nd Edition, Undergraduate Texts in Mathematics. Springer, New York.

Steinberg, M.S., 1962a. On the mechanism of tissue reconstruction of tissues by dissociated cells, III. Free energy relations and the reorganization of fused, heteronomic tissue fragments. Proc. Natl Acad. Sci. USA 48 (10), 1769–1776.

Steinberg, M.S., 1962b. On the mechanism of tissue reconstruction by dissociated cells, I. Population kinetics, differential adhesiveness, and the absence of directed migration. Proc. Natl Acad. Sci. U.S.A. 48 (9), 1577–1582.

Steinberg, M.S., 1963. Reconstruction of tissues by dissociated cells. Science 141 (3579), 401–408.

Steinberg, M.S., 1975. Reconstruction of tissues by dissociated cells. In: Mostow, G.D. (Ed.), Mathematical Models for Cell Rearrangement. Yale University Press, New Haven, CT, pp. 82–99 (Chapter 6).

Stott, E.L., Britton, N.F., Glazier, J.A., Zajac, M., 1999. Stochastic simulation of benign avascular tumour growth using the Potts Model. Math. Comput. Model. 30, 183–198.

Upadhyaya, A., 2000. Thermodynamic and fluid properties of properties of cells, tissues and membranes. Ph.D. Thesis, University of Notre Dame, Notre Dame, Indiana.

Weliky, M., Minsuk, S., Keller, R., Oster, G., 1991. Notochord morphogenesis in *Xenopus laevis*: simulation of cell behavior underlying tissue convergence and extension. Development 113 (4), 1231–1244.

Winklbauer, R., Nagel, M., 1991. Directional mesoderm cell migration in the *Xenopus gastrula*. Dev. Bio. 148, 573–589.

Wolpert, L., Beddington, R., Brockes, J., Jessel, T., Peter, L., Meyerowitz, E., 1998. Principles of Development. Oxford University Press, New York.

Zajac, M., 2002. Modeling convergent extension by way of anisotropic differential adhesion. Ph.D. Thesis, University of Notre Dame, Notre Dame, Indiana.

Zajac, M., Jones, G.L., Glazier, J.A., 2000. Model of convergent extension in animal morphogenesis. Phys. Rev. Lett. 85 (9), 2022–2025.